C.P. No. 1007

C.P. No. 1007

MINISTRY OF TECHNOLOGY

AERONAUTICAL RESEARCH COUNCIL

CURRENT PAPERS

Low-Speed Measurements of Skin Friction on a Large Half-Model Slender Wing

by

L. A. Wyatt and L F. East

LONDON: HER MAJESTY'S STATIONERY OFFICE

1968

PRICE 4s 6d NET

U.D.C. 532.526.7 : 533.693.3 : 533.6.071 : 533.6.011.32/34

C.P. No. 1007*
August 1967

LOW-SPEED MEASUREMENTS OF SKIN FRICTION ON A LARGE HALF-MODEL SLENDER WING

by

L. A. Wyatt
L. F. East

SUMMARY

Skin-friction measurements have been made on a half-model slender wing of 24 ft root chord at low subsonic speeds. The maximum root-chord Reynolds number was 30×10^6. The measurements were made using surface pitot-tubes formed by magnetically attaching razor-blade segments to the model surface. The results show that high levels of skin friction are present beneath the leading-edge vortex and are correlated satisfactorily with previous results obtained at lower Reynolds numbers.

---

* Replaces R.A.E. Technical Report 67209 - A.R.C. 29755

CONTENTS

1 INTRODUCTION

Ref.1 describes comprehensive low-speed measurements of the skin-friction distribution over the upper surface of a slender wing (rhombic cone) at incidence, using the razor blade technique with the blades retained by magnets.

During a subsequent investigation of surface pressure fluctuations on a slender wing, a half-model wing of 24 ft root chord was built with the same plan-form as the rhombic cone and the opportunity has been taken to repeat some of the skin-friction measurements at the higher Reynolds number available.

The experiments were made in the R.A.E. Bedford 13 ft × 9 ft low-speed wind-tunnel during Spring, 1966.

2 EXPERIMENTAL DETAILS

2.1 Model details

The measurements were made on the plane upper surface of a 'flat-plate' delta half-wing of full aspect ratio unity (leading-edge sweep 76°) with a basic root chord of 24 ft. The model consisted of a steel framework covered by 1 inch thick plywood skins with a smooth matt black finish and had a constant thickness of 6 inches except near the leading and trailing edges which were bevelled on the under-side to sharp edges with an included angle of about 34° (Fig.1). The wing was mounted vertically from the floor turn-table of the 13 ft × 9 ft tunnel (see Fig.2) with the axis of rotation at the position of the estimated centre of pressure (60% root chord). Two alternative nose sections were provided. The leading edge apex of nose A was at floor level, whereas the apex of nose B was 3 inches above floor level (see Fig.1) and consequently was outside the 2 inch thick floor boundary layer. The corresponding model root chords and semi-spans were therefore c_A = 24 ft, s_A = 6 ft and c_B = 23 ft, s_B = 5.75 ft. A nominal clearance of 0.25 inch was left between the root of the model and the tunnel floor: this gap was sealed for nose B but was left open for nose A.

For the skin-friction measurements, two 4 inch wide brass plates each incorporating a row of magnets were flush mounted across the local span of the model in the upper surface. The plates were placed 9 ft and 18 ft back from the basic leading-edge apex, giving non-dimensional positions

x/c_A = 0.375, 0.750 and x/c_B = 0.348, 0.739 for noses A and B respectively (see Fig.1). There were 18 and 30 measuring points respectively in the forward and rear plates.

2.2 Experimental procedure

The experiments were conducted at nominal wind speeds of 150 and 200 ft/sec, giving a maximum Reynolds number based on root chord of 30×10^6 (cf. a maximum of 9×10^6 in previous tests[1]) and at incidences between -2° and 12° (uncorrected for wall constraint).

The skin friction was measured indirectly using small razor blade segments attached magnetically to the model surface. The segments were 0.005 inch high and were aligned with the surface flow direction, which was determined for each incidence by the oil flow visualisation technique. The details of the razor blade method used, including the calibration, are exactly the same as described in Ref.1.

Measurements were made with both nose shapes. In the previous tests[1], distributed roughness had been applied at the apex to eliminate regions of laminar flow beneath the vortices near the nose of the model and so ensure a conical surface oil-flow pattern. On the half-model, roughness was needed with nose B, but not with nose A - presumably the turbulence level in the 2 inch thick floor boundary layer was a sufficient trigger in the latter case.

3 DISCUSSION OF RESULTS

3.1 Oil flow patterns

The oil flow visualisation technique was used to pick out the dominant features of the surface flow beneath the vortex and so give a clear indication as to whether the flow could be regarded as conical or not. The flow tests showed that, at incidences of 0° and below, the leading-edge vortex was stronger over the forward portion of the model and conical flow was certainly not present. This was expected as the model itself was not conical. However at higher incidences there was no detectable influence of the model shape on the surface flow patterns which then appeared to be conical. Although a limited comparison only of the static pressure distributions at the two chordwise stations is available, the flow measurements show that, at least for incidences above 2°, a reasonably conical flow field existed.

Oil flow patterns were also taken at the wing-floor junction to determine the corner flow with the gap between the wing and floor both open and closed. As nose A was tested with the gap open whereas nose B was used with the gap sealed it is not entirely possible to separate the effects of the gap from those due to the different nose shapes. The oil flow patterns showed that with nose A at incidence, flow through the open gap interacted with the streamwise flow to generate a weak vortex lying in the wing-floor junction (Fig.3). The small vortex formed on the section of leading edge between the apex of nose B and the floor, which had the same direction of rotation as the vortex formed by the gap flow, did not persist far downstream and had no visible effect on the flow in the wing-floor junction which appeared to be parallel to the junction. It is concluded that any difference between the two configurations detected at a point distant from the apex and near the floor is more likely to be due to the gap than to the different apex configurations.

3.2 Static pressure measurements

The static pressure distributions across the model span are shown in Fig.4 for $\alpha = 6°$ and $10°$ and the complete results are tabulated in Table 1 together with the skin-friction coefficients. In both Table 1 and Figs.4, 5 and 6, y and s_x are measured, with nose B fitted, from the implied centre line of the complete model which passes through the apex (see Fig.1). This 3 inch shift in zero affects the values of y/s_x and it appears that the suction peaks shown in Fig.4 for different nose shapes and measuring stations line up more closely if the zero shift is ignored. Correlation of the positions of the suction peaks can also be achieved between noses A and B by increasing the values of α for nose B by about one degree. This is most clearly seen in Fig.6 which summarises the characteristics of the suction and skin-friction peaks. Although the addition of $1°$ improves the correlation of the position and magnitude of the suction peak for noses A and B, the correlation of the position of the maximum skin friction is little affected and that of its magnitude is worsened. It is probable that the effect of the gap is to lower the loading of the whole wing by an amount equivalent to a reduction of incidence of about one degree, but that changes in the cross flow produced by the gap, upon which the skin friction is strongly dependent, cannot be related in the same simple way.

In addition to the main suction peak situated at $y/s_x \approx 0.7$ a much smaller peak shows up clearly at $y/s_x \approx 0.93$ which coincides with the secondary vortex as shown by the oil flow patterns.

3.3 Skin-friction measurements

The spanwise skin-friction distributions are shown in Fig.5 and are tabulated in Table 1. The skin-friction coefficient C_f is based upon the free-stream kinetic pressure. In Fig.5 the ratio C_f/C_{f_x} is plotted in which C_{f_x} is a two-dimensional skin-friction coefficient based upon the Reynolds number appropriate to the distance, x (see Fig.1), of the measuring station from the leading edge apex. The expression for C_{f_x} used is[2],

$$C_{f_x} = 0.288 \, (\mathrm{Log}_{10} R_x)^{-2.45} \quad .$$

In Ref.1 it was found that the quantity C_f/C_{f_x} satisfactorily correlated the data for different Reynolds numbers at a given incidence and Fig.5 shows that the present results also correlate. The previously established shape[1] of the skin-friction distribution is confirmed, though for $\alpha \geq 6^\circ$ the graphs show differences in the skin friction measured over the inboard half of the model which are attributed to the flow through the gap at the root. The higher values of skin friction obtained with the gap open are consistent with the slight divergence of the boundary layer over the inboard area of the model which is induced by the vortex (Fig.3) at the model root.

Due to the presence of camber on the half model and the different wall constraint corrections for the two models, there is not an exact correspondence between incidences and direct comparison of the present results with those of Ref.1 is not possible. However, as shown in Fig.6, if the incidence of the complete model is decreased by 3°, good agreement is obtained as regards the dominant features of the skin friction and pressure distributions. Of this 3° incidence adjustment, about 2° can be regarded as allowing for the no-lift angle of the half-wing and the remaining 1° as a rough mean of the different wall corrections to incidence over the range of incidence covered. In this latter respect, it may be noted that $S/C = 0.08$ and $c/h = 0.67$ for the complete model, where $S/C = 0.65$ and $c_A/h = 1.85$ for the half model! (S is the wing area, C is the tunnel cross-sectional area and h is the

tunnel dimension in the incidence plane.) In Fig.6, the peak value of C_f/C_{f_x} and its spanwise location y/s_x have been selected as the main features of the skin-friction distribution and are plotted against incidence. The incidences of the present tests have been left unchanged and those of Ref.1 have had 3° subtracted from them. The two sets of data are then in good agreement and a similar comparison of the peak C_p and its spanwise location bears out this result. The variation of $(C_f/C_{f_x})_{max}$ and $(C_f/C_{f_x})_{min}$ with incidence can also be eliminated by basing the skin-friction coefficient on the local kinetic pressure (C_{f_q}) and the resultant values then agree with Ref.1. This agreement for the case of $(C_{f_q}/C_{f_x})_{max}$ follows from the agreement shown in Fig.6 since,

$$(C_{f_q}/C_{f_x})_{max} \approx (C_f/C_{f_x})_{max}/(1 - C_{p_{max}}) \quad .$$

Considering the reservations made regarding the precise nature of the half-model flow field and the differing camber and thickness distributions of the two models, the agreement is very satisfactory.

4 CONCLUSIONS

Measured skin-friction distributions on a large half-model of a slender wing at Reynolds numbers up to 30×10^6 show good agreement with previous results from a complete model of slightly different geometry at lower Reynolds numbers. It is probable that data will be forthcoming from the HP 115 research aircraft which would extend these results to still higher Reynolds numbers.

Table 1

SKIN-FRICTION AND PRESSURE COEFFICIENTS

Nose A $x/c_o = 0{\cdot}75$ U = 200 ft/sec

y/s_x	$\alpha = 0°$		$\alpha = 2°$		$\alpha = 4°$		$\alpha = 6°$	
	$10^3\ C_f$	$-C_p$	$10^3\ C_f$	$-C_p$	$10^3\ C_f$	$-C_p$	$10^3\ C_f$	$-C_p$
0·109	2·3	0·035	2·3	0·051	2·5	0·069	2·8	0·089
0·184	2·5	0·037	2·3	0·053	2·5	0·070	2·8	0·090
0·258	2·6	0·036	2·5	0·052	2·8	0·069	3·0	0·088
0·332	2·8	0·038	2·6	0·053	2·6	0·070	3·1	0·089
0·407	3·0	0·038	2·9	0·052	2·9	0·066	3·4	0·085
0·444	3·1	0·036	2·7	0·050	3·0	0·063	3·3	0·083
0·481	2·9	0·034	2·8	0·045	3·0	0·057	3·4	0·084
0·518	3·0	0·034	3·1	0·044	3·1	0·054	3·6	0·092
0·555	2·7	0·035	3·1	0·042	3·2	0·055	3·6	0·114
0·592	2·8	0·036	3·1	0·037	3·5	0·063	4·1	0·157
0·630	2·8	0·035	3·4	0·034	3·7	0·085	5·0	0·230
0·648	2·9	0·035	3·6	0·035	4·1	0·113	4·7	0·281
0·667	2·9	0·035	3·4	0·039	4·4	0·143	4·4	0·336
0·685	3·1	0·034	3·5	0·051	4·3	0·192	5·4	0·391
0·704	3·1	0·035	3·9	0·071	4·6	0·234	5·9	0·441
0·722	3·1	0·036	4·3	0·103	5·0	0·291	5·6	0·477
0·741	3·1	0·037	4·2	0·139	5·0	0·340	5·4	0·490
0·760	3·2	0·039	4·2	0·178	5·2	0·375	4·9	0·480
0·778	3·2	0·046	4·6	0·215	5·2	0·383	4·7	0·445
0·797	3·2	0·048	4·3	0·236	4·7	0·355	4·0	0·386
0·815	3·1	0·049	4·2	0·231	3·6	0·297	3·0	0·320
0·834	2·8	0·049	3·5	0·204	2·5	0·237	2·0	0·290
0·852	3·1	0·049	2·9	0·169	1·8	0·220	2·1	0·285
0·871	3·0	0·060	2·1	0·149	2·1	0·218	2·4	0·284
0·890	2·9	0·069	1·9	0·145	2·1	0·218	2·2	0·282
0·908	2·8	0·075	2·3	0·144	2·9	0·220	3·1	0·288
0·927	2·6	0·074	3·0	0·143	3·2	0·219	3·4	0·296
0·945	2·3	0·073	2·8	0·138	3·6	0·210	3·7	0·284
0·964	2·2	0·075	2·9	0·135	3·1	0·202	3·5	0·267
0·983	2·0	0·075	2·6	0·132	3·0	0·196	3·2	0·258

Table 1 (contd)

Nose A $x/c_o = 0{\cdot}75$ U = 150 ft/sec

y/s_x	$\alpha = 8°$		$\alpha = 10°$		$\alpha = 12°$	
	$10^3 C_f$	$-C_p$	$10^3 C_f$	$-C_p$	$10^3 C_f$	$-C_p$
0·109	3·3	0·123	3·4	0·147	3·5	0·188
0·184	3·4	0·123	3·5	0·138	3·5	0·173
0·254	3·5	0·121	3·5	0·141	3·7	0·184
0·332	3·5	0·124	3·8	0·155	3·9	0·209
0·407	3·6	0·129	4·1	0·181	4·3	0·266
0·444	3·8	0·136	4·3	0·206	4·6	0·315
0·481	4·0	0·155	4·5	0·251	5·2	0·377
0·518	4·4	0·191	4·6	0·318	5·3	0·468
0·555	4·6	0·255	5·2	0·412	6·3	0·586
0·592	4·8	0·343	5·4	0·525	6·7	0·704
0·630	5·6	0·458	6·5	0·639	6·8	0·806
0·648	5·9	0·519	6·7	0·691	7·0	0·846
0·667	6·5	0·575	6·2	0·730	6·9	0·872
0·685	6·4	0·616	6·5	0·749	6·9	0·880
0·704	6·3	0·645	6·4	0·753	6·6	0·866
0·722	5·9	0·648	5·9	0·736	6·2	0·835
0·741	5·5	0·628	5·0	0·694	5·9	0·788
0·760	5·0	0·586	4·6	0·639	4·9	0·727
0·778	4·5	0·526	4·4	0·575	4·5	0·659
0·797	3·7	0·456	3·4	0·506	3·8	0·590
0·815	2·8	0·403	2·6	0·462	2·7	0·544
0·834	2·0	0·388	1·8	0·449	2·0	0·529
0·852	2·3	0·382	2·3	0·444	2·0	0·519
0·871	2·5	0·382	2·6	0·446	3·0	0·522
0·890	2·2	0·380	2·2	0·444	2·5	0·522
0·908	3·1	0·386	3·1	0·449	3·1	0·522
0·927	3·7	0·398	3·9	0·464	3·7	0·537
0·945	4·1	0·395	4·0	0·465	4·4	0·546
0·964	4·1	0·369	4·2	0·441	4·3	0·528
0·983	4·1	0·356	4·2	0·418	4·2	0·494

Table 1 (contd)

Nose B $x/c_o = 0.74$ U = 150 ft/sec

y/s_x	$\alpha = 2°$		$\alpha = 4°$		$\alpha = 6°$		$\alpha = 8°$	
	$10^3 C_f$	$-C_p$	$10^3 C_f$	$-C_p$	$10^3 C_f$	$-C_p$	$10^3 C_f$	$-C_p$
0·056	2·4	0·061	2·7	0·080	2·5	0·099	2·7	0·122
0·135	2·5	0·060	2·5	0·080	2·5	0·098	2·8	0·121
0·214	2·5	0·060	2·7	0·077	2·7	0·097	2·8	0·121
0·293	2·2	0·050	1·9	0·048	2·6	0·082	2·8	0·107
0·371	2·9	0·059	2·6	0·055	3·0	0·095	2·9	0·136
0·411	2·9	0·056	3·0	0·071	3·1	0·095	3·5	0·148
0·450	3·2	0·054	2·6	0·048	3·2	0·100	3·9	0·172
0·490	3·2	0·052	2·7	0·047	3·6	0·114	3·7	0·215
0·529	3·2	0·049	3·6	0·070	3·7	0·143	4·3	0·283
0·568	3·3	0·045	3·8	0·085	4·0	0·199	4·6	0·379
0·608	3·4	0·044	3·9	0·122	4·3	0·287	5·0	0·495
0·627	3·6	0·046	4·3	0·154	4·9	0·345	5·4	0·553
0·647	3·7	0·055	4·2	0·197	5·0	0·407	5·7	0·607
0·667	3·9	0·075	4·7	0·250	5·6	0·468	5·9	0·649
0·686	4·0	0·104	4·7	0·311	5·5	0·519	5·9	0·668
0·706	4·3	0·149	5·5	0·371	5·5	0·552	6·0	0·673
0·726	4·5	0·191	5·2	0·419	5·0	0·561	5·2	0·652
0·745	4·3	0·240	5·3	0·444	4·7	0·540	4·9	0·608
0·765	4·7	0·285	4·8	0·436	4·3	0·494	4·3	0·553
0·785	4·7	0·302	4·6	0·392	3·7	0·427	3·4	0·479
0·804	4·4	0·284	3·5	0·323	2·9	0·359	2·7	0·422
0·824	3·5	0·236	2·4	0·267	1·8	0·331	1·8	0·401
0·844	2·5	0·191	1·8	0·255	1·9	0·325	2·1	0·396
0·863	2·1	0·154	2·4	0·221	2·8	0·284	2·8	0·348
0·883	2·1	0·177	2·3	0·253	2·0	0·324	2·0	0·393
0·903	2·6	0·179	3·1	0·259	2·7	0·330	2·7	0·398
0·922	3·1	0·176	3·3	0·260	3·2	0·339	3·6	0·413
0·942	3·1	0·167	3·5	0·251	3·4	0·329	3·9	0·413
0·962	3·0	0·162	3·3	0·235	3·6	0·309	3·9	0·390
0·981	2·8	0·159	3·0	0·230	3·5	0·298	3·8	0·370

Table 1 (contd)

Nose B $x/c_o = 0{\cdot}35$ U = 150 ft/sec

y/s_x	$\alpha = 2°$		$\alpha = 6°$		$\alpha = 10°$	
	$10^3 C_f$	$-C_p$	$10^3 C_f$	$-C_p$	$10^3 C_f$	$-C_p$
0·079	2·8	0·053	2·9	0·111	3·3	0·201
0·163	2·9	0·051	2·9	0·109	3·6	0·203
0·247	3·3	0·046	3·3	0·105	3·6	0·210
0·331	3·1	0·042	3·4	0·101	4·0	0·232
0·415	3·5	0·042	3·6	0·108	4·7	0·303
0·457	3·6	0·040	3·8	0·116	6·4	0·365
0·499	3·7	0·037	4·2	0·139	5·5	0·457
0·541	4·1	0·029	4·6	0·180	6·1	0·573
0·583	4·5	0·031	5·1	0·264	6·9	0·711
0·625	4·5	0·040	5·7	0·367	7·0	0·821
0·667	5·0	0·088	6·2	0·509	7·3	0·881
0·709	5·4	0·185	6·2	0·583	6·0	0·854
0·751	5·8	0·297	5·4	0·542	4·7	0·735
0·793	4·8	0·274	3·3	0·413	3·2	0·613
0·835	2·8	0·179	2·0	0·354	2·0	0·564
0·877	2·4	0·169	2·1	0·349	2·4	0·558
0·919	3·8	0·169	4·2	0·370	4·1	0·578
0·961	3·8	0·153	4·2	0·334	4·8	0·567

SYMBOLS

x	distance behind leading-edge apex
y	spanwise distance from wing root
c	root chord
s	semi-span
s_x	local semi-span at station x
α	incidence
U	tunnel free-stream velocity
C_p	pressure coefficient
C_f	skin-friction coefficient
C_{f_q}	skin-friction coefficient based on local kinetic pressure
C_{f_x}	skin-friction coefficient in two-dimensional flow
S	wing area
C	tunnel cross-sectional area
h	tunnel dimension in incidence plane
$( )_{A,B}$	suffices referring to noses A and B respectively

REFERENCES

No.	Author	Title, etc.
1	L.A. Wyatt L.F. East	Low-speed measurements of skin friction on a slender wing. A.R.C. R. & M. 3499, 1966
2	R.J. Monaghan	Formulae and approximations for aerodynamic heating rates in high speed flight. A.R.C. C.P. 360, 1956

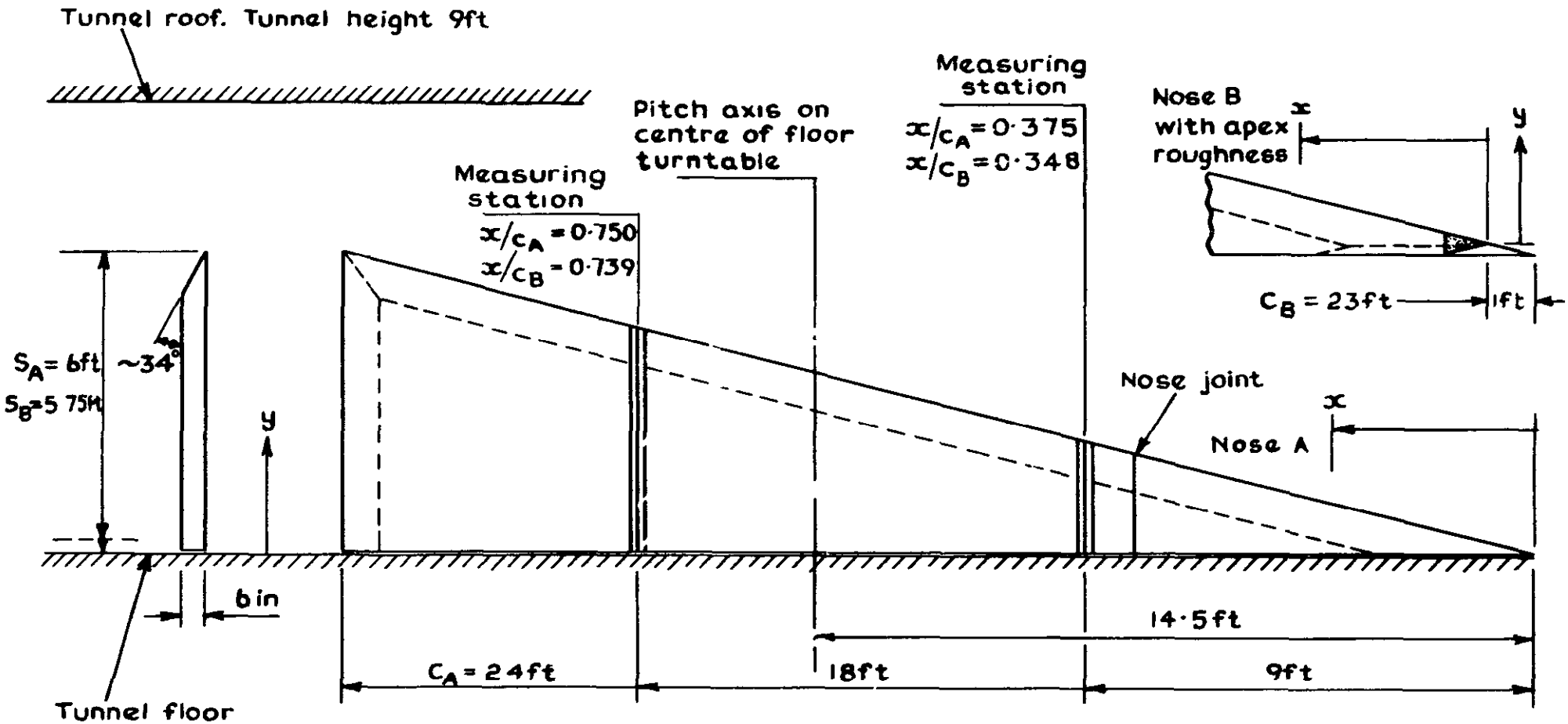

Fig. 1 G.A. of slender wing half-model

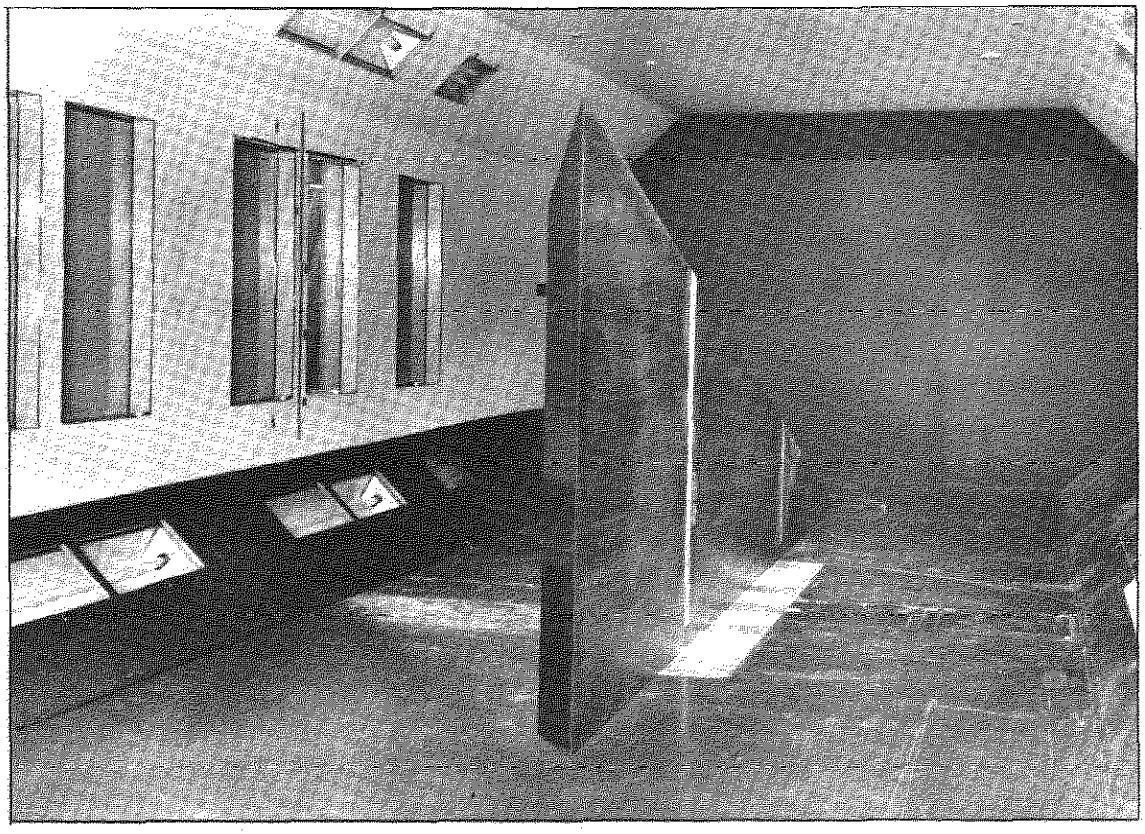

Fig.2 Model in 13ft. X 9ft. tunnel

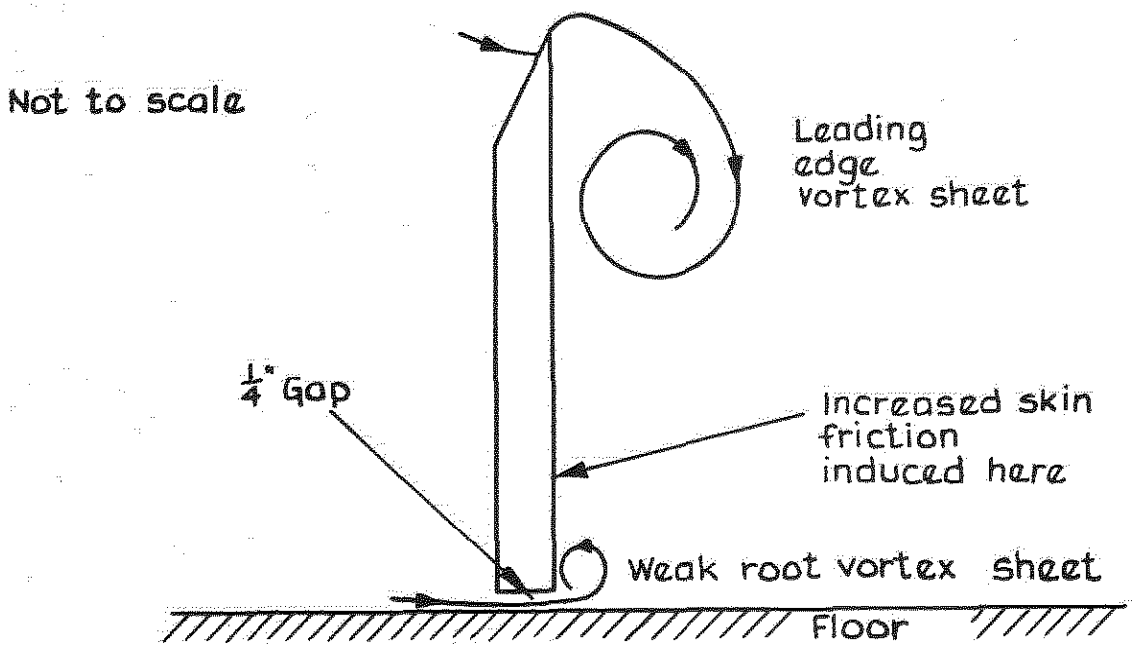

Fig.3 Effect of flow through gap at wing root

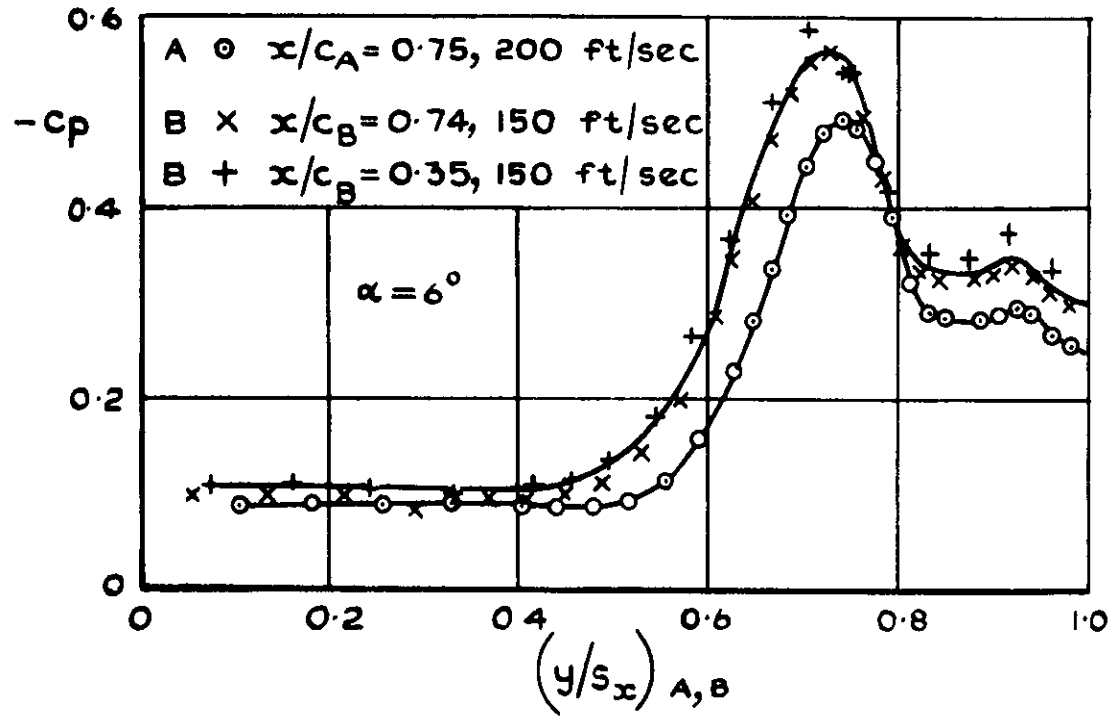

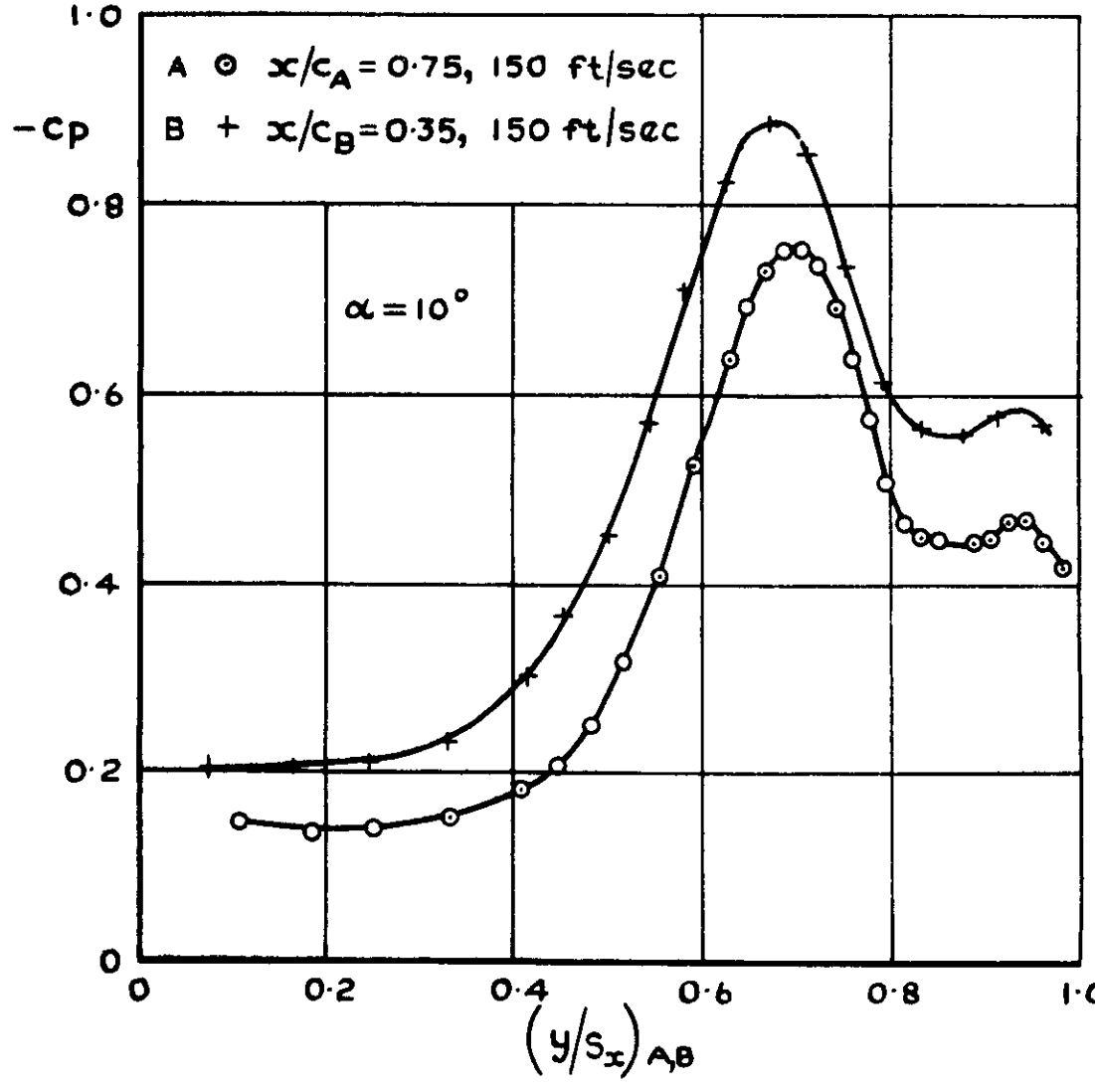

Fig. 4 Distribution of C_p over upper surface at $\alpha = 6°, 10°$

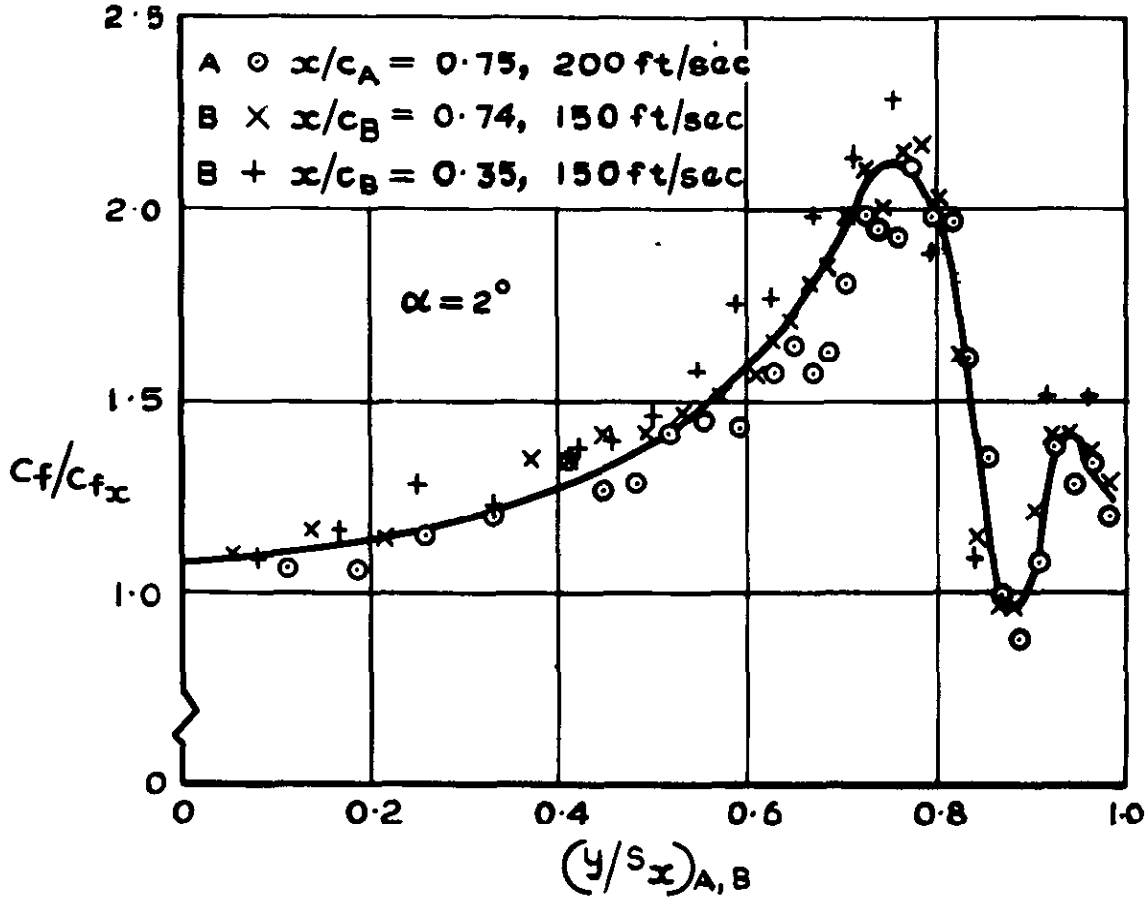

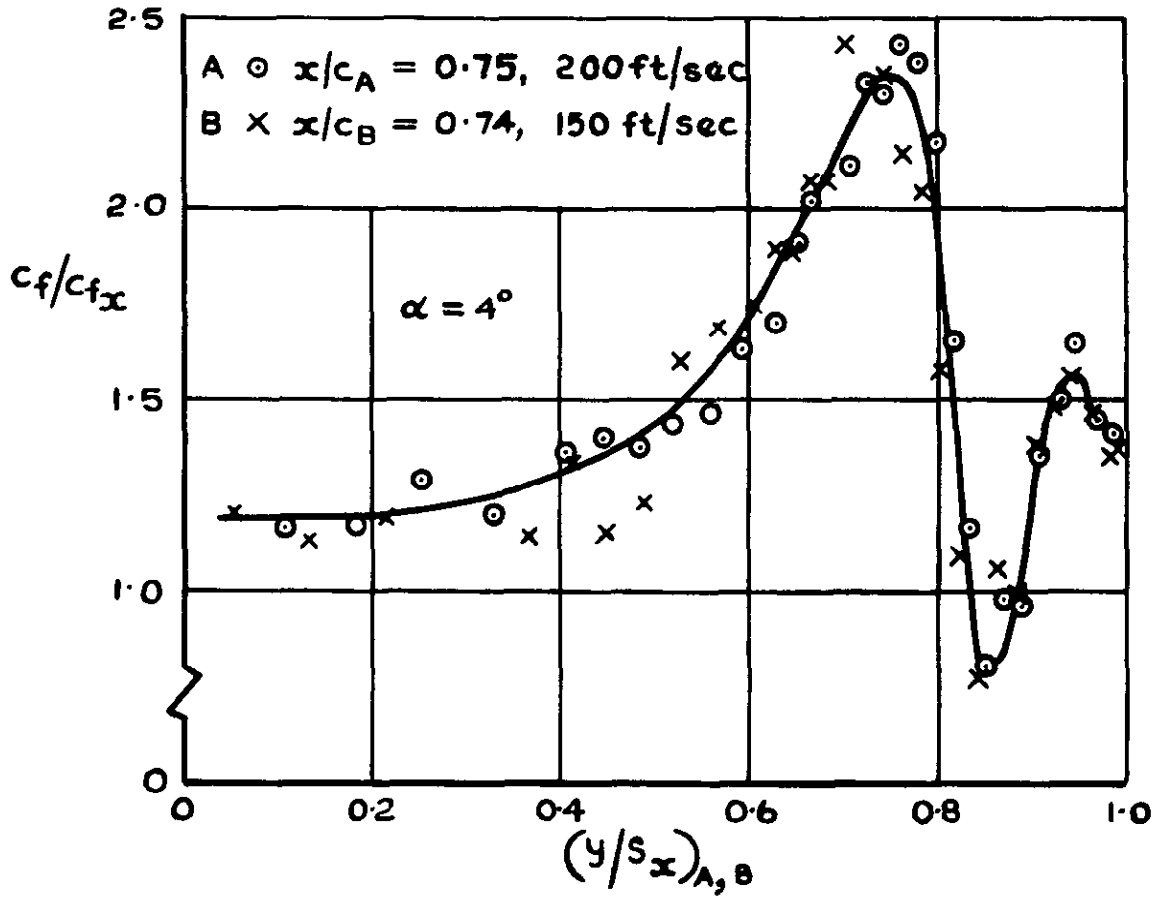

Fig. 5 Distribution of C_f/C_{f_x} over upper surface at $\alpha = 2°, 4°$

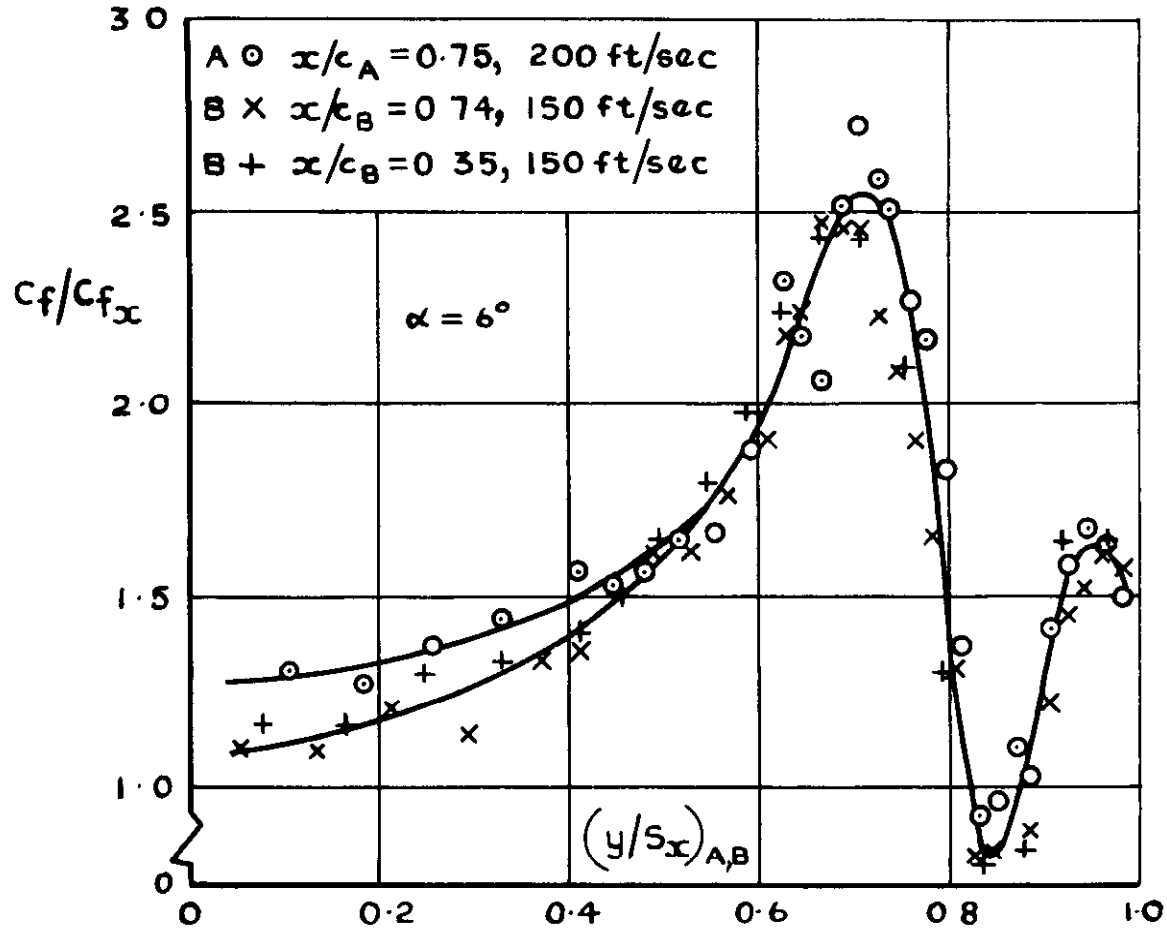

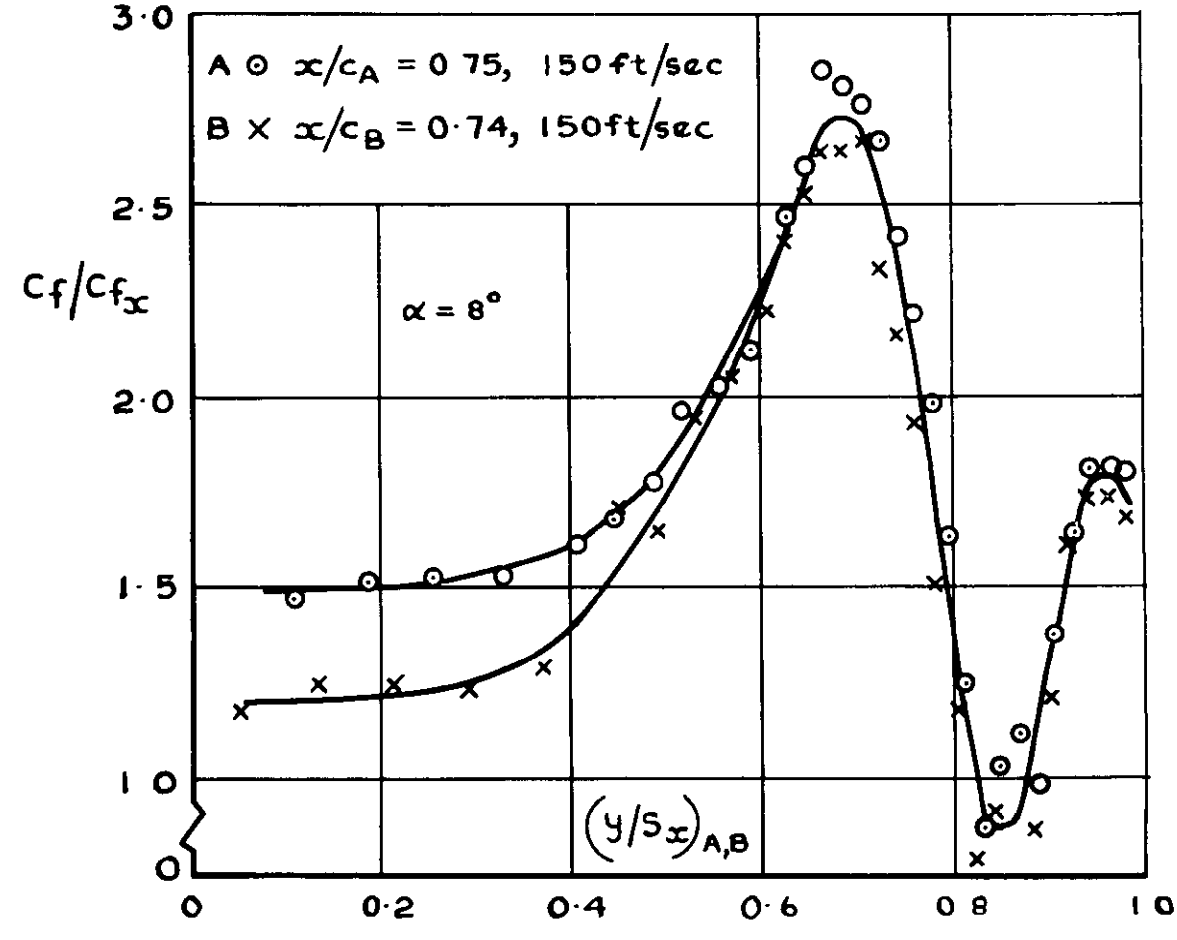

Fig. 5 contd Distribution of C_f/C_{fx} over upper surface at $\alpha = 6°, 8°$

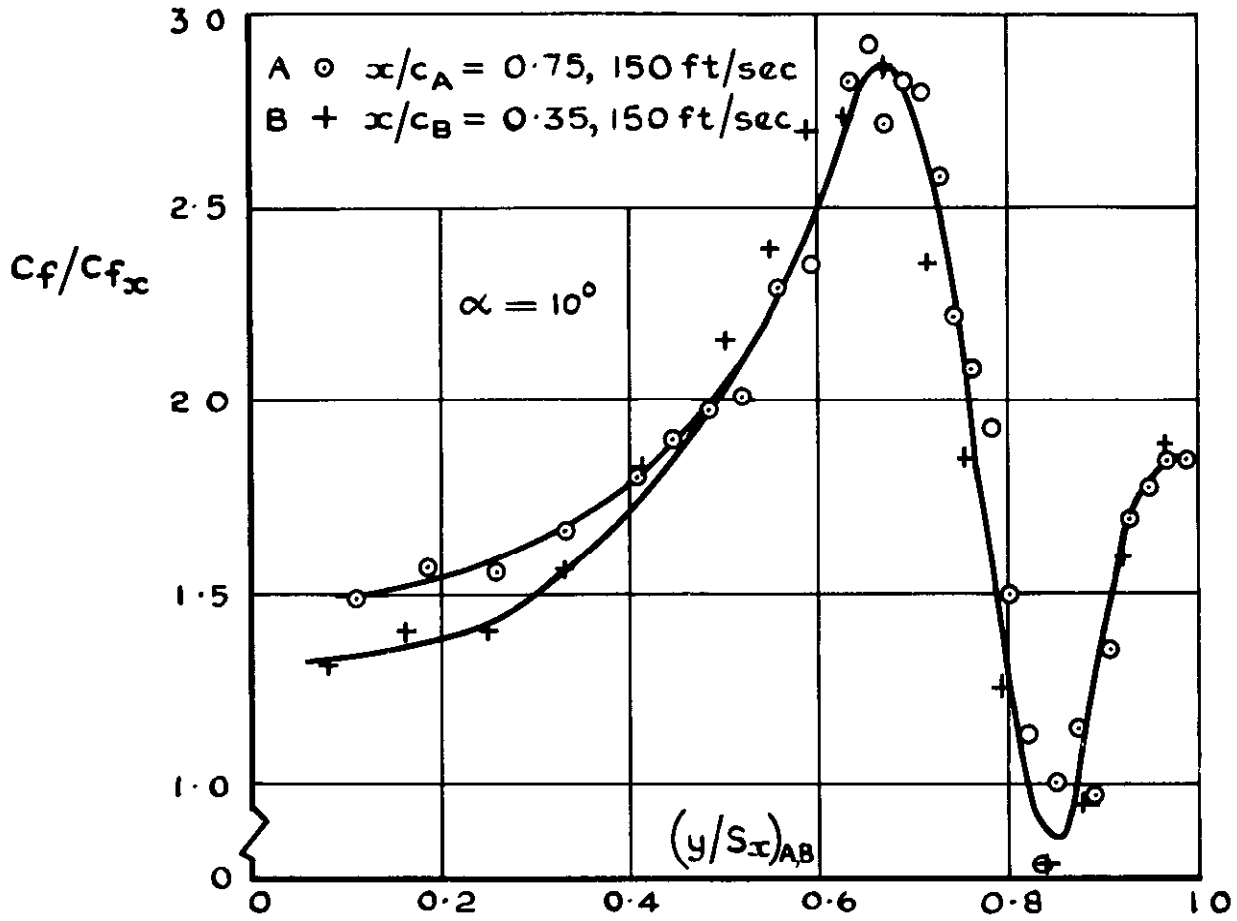

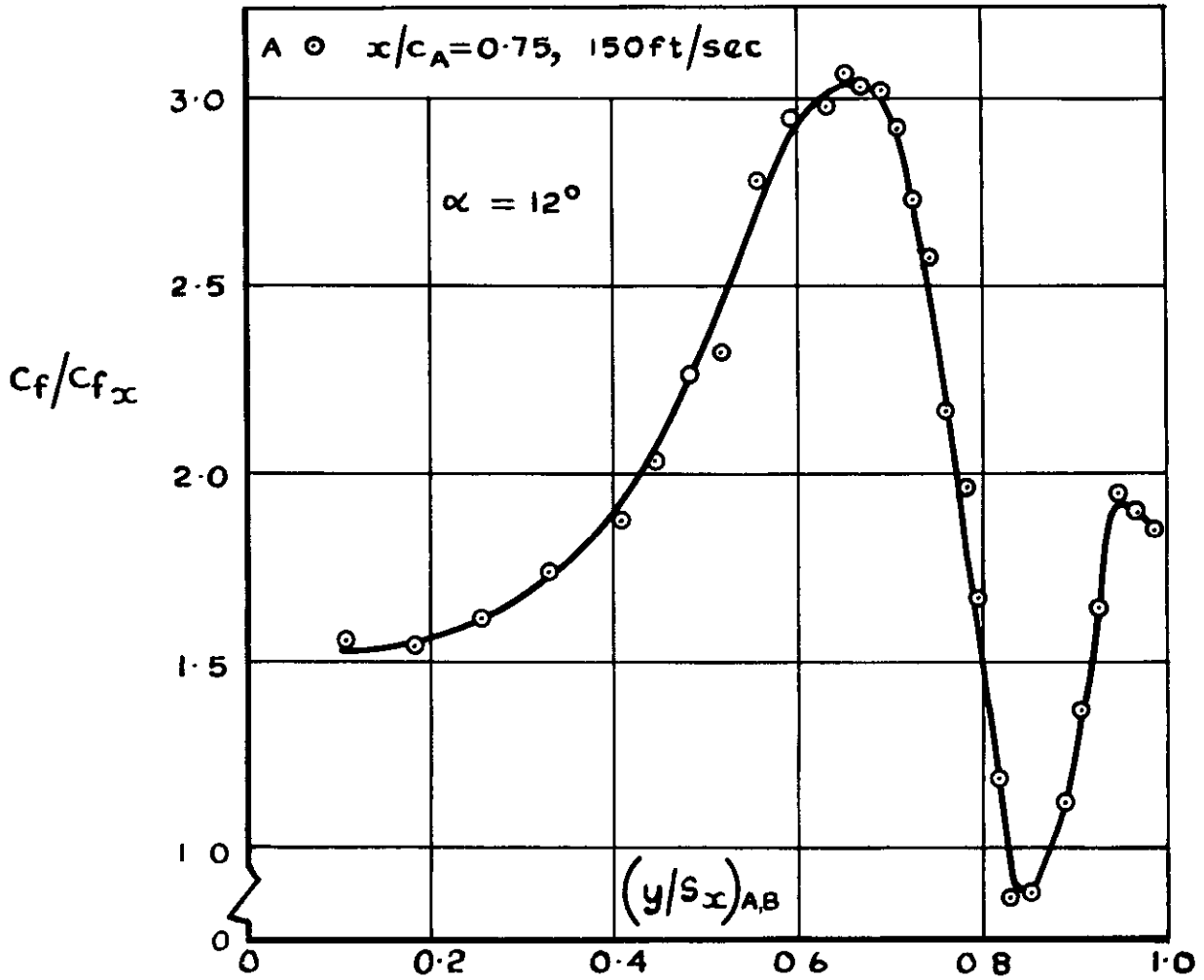

Fig. 5 concld Distribution of C_f/C_{f_x} over upper surface at $\alpha = 10°, 12°$

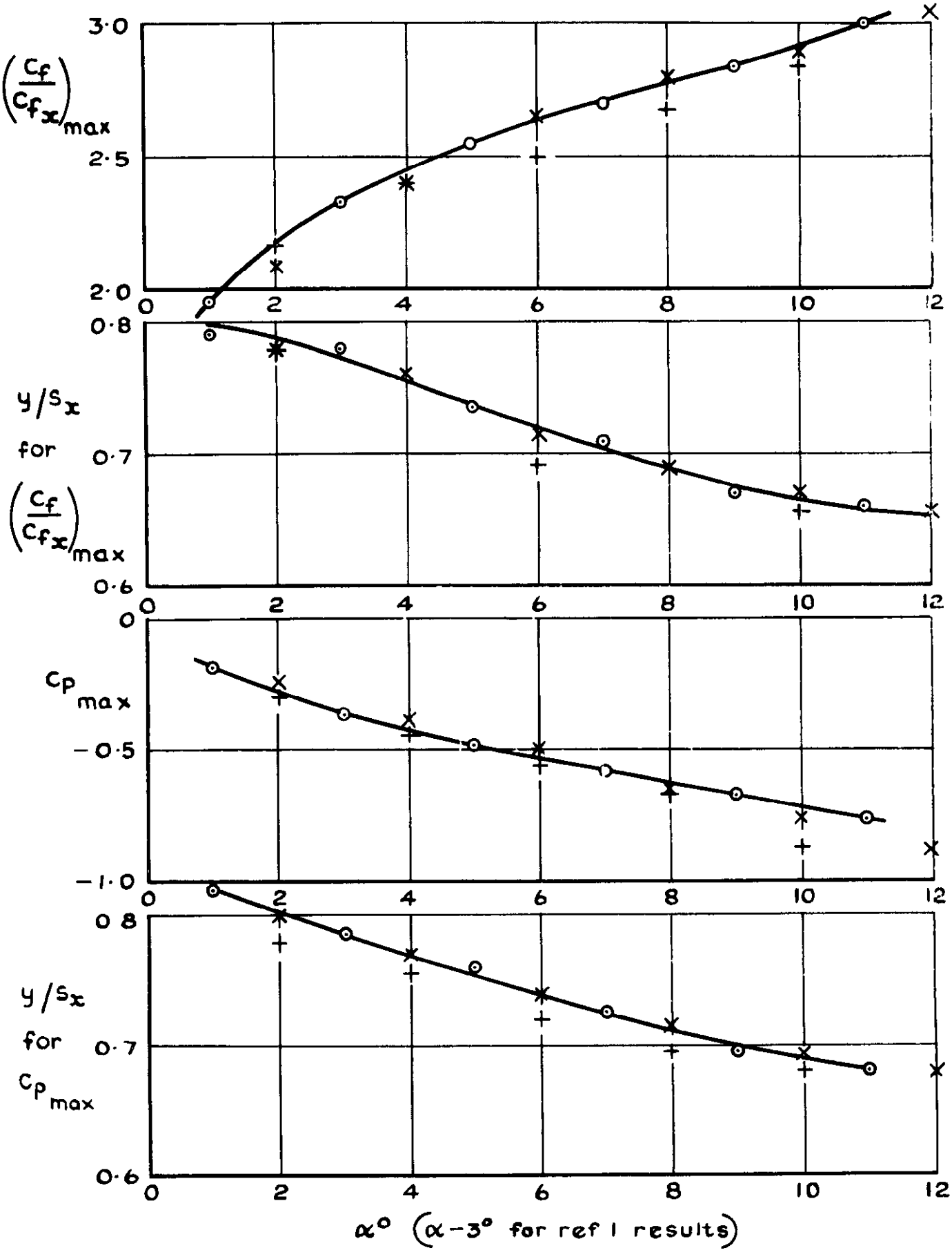

Fig. 6 Comparison with test results on Rhombic cone

Printed in England for Her Majesty's Stationery Office by the Royal Aircraft Establishment Farnborough. Dd 135845 K 3

A.R.C. C.P. No.1007
August 1967

Wyatt, L.A.
East, L.F.

532.526.7 :
533.693.3 :
533.6.071 :
533.6.011.32/34

LOW-SPEED MEASUREMENTS OF SKIN FRICTION ON A LARGE HALF-MODEL SLENDER WING

Skin-friction measurements have been made on a half-model slender wing of 24 ft root chord at low subsonic speeds. The maximum root-chord Reynolds number was 30 x 10^6. The measurements were made using surface pitot-tubes formed by magnetically attaching razor-blade segments to the model surface. The results show that high levels of skin friction are present beneath the leading-edge vortex and are correlated satisfactorily with previous results obtained at lower Reynolds numbers.

A.R.C. C.P. No.1007
August 1967

Wyatt, L.A.
East, L.F.

532.526.7 :
533.693.3 :
533.6.071 :
533.6.011.32/34

LOW-SPEED MEASUREMENTS OF SKIN FRICTION ON A LARGE HALF-MODEL SLENDER WING

Skin-friction measurements have been made on a half-model slender wing of 24 ft root chord at low subsonic speeds. The maximum root-chord Reynolds number was 30 x 10^6. The measurements were made using surface pitot-tubes formed by magnetically attaching razor-blade segments to the model surface. The results show that high levels of skin friction are present beneath the leading-edge vortex and are correlated satisfactorily with previous results obtained at lower Reynolds numbers.

A.R.C. C.P. No.1007
August 1967

Wyatt, L.A.
East, L.F.

532.526.7 :
533.693.3 :
533.6.071 :
533.6.011.32/34

LOW-SPEED MEASUREMENTS OF SKIN FRICTION ON A LARGE HALF-MODEL SLENDER WING

Skin-friction measurements have been made on a half-model slender wing of 24 ft root chord at low subsonic speeds. The maximum root-chord Reynolds number was 30 x 10^6. The measurements were made using surface pitot-tubes formed by magnetically attaching razor-blade segments to the model surface. The results show that high levels of skin friction are present beneath the leading-edge vortex and are correlated satisfactorily with previous results obtained at lower Reynolds numbers.

DETACHABLE ABSTRACT CARDS

Published by
HER MAJESTY'S STATIONERY OFFICE

To be purchased from
49 High Holborn, London W C 1
423 Oxford Street, London W 1
13A Castle Street, Edinburgh 2
109 St Mary Street, Cardiff
Brazennose Street, Manchester 2
50 Fairfax Street, Bristol 1
258-259 Broad Street, Birmingham 1
7-11 Linenhall Street, Belfast 2
or through any bookseller

S.O. CODE No. 23-9018-7